Flutter Analysis of Floating Horizontal-axis Wind Turbine Blades

Saeid Fadaei (saeidfadaeinaeini@cmail.carleton.ca)
Carleton University
Abbas Mazidi
Yazd University
Fred Afagh
Carleton University
Robert G. Langlois
Carleton University

Research Article

Keywords: Floating wind turbine, Flutter, Non-uniform blade

Posted Date: June 8th, 2022

DOI: https://doi.org/10.21203/rs.3.rs-1738821/v1

Declaration of interests

☒ The authors declare that they have no known competing financial interests or personal relationships that could have appeared to influence the work reported in this paper.

☐The authors declare the following financial interests/personal relationships which may be considered as potential competing interests:

Flutter Analysis of Floating Horizontal-axis Wind Turbine Blades

S. Fadaei[*1], A. Mazidi[2], F. Afagh, R. G. Langlois[1]

[1]Department of Mechanical and Aerospace Engineering, Carleton University, Ottawa, Canada

[2]Department of Mechanical Engineering, Yazd University, Yazd, Iran

Abstract

In this study, flutter of blades in floating horizontal-axis wind turbines is investigated. The blade is modeled as a non-uniform Euler-Bernoulli beam in bending and torsion, which can experience large deflections. The discretized form of the aeroelastic governing equations of the blade is obtained by combining blade element momentum theory (BEM) and geometrically exact beam theory (GEBT). To emulate the true physical and geometrical properties of the blade, for each property, a mathematical function that has been fit to the series of data points corresponding to the NREL 5 MW turbine blade is constructed and used in the aeroelastic governing equations. Numerical results are compared with the results obtained from the ABAQUS software and good agreement is observed. Results are presented for both parked and operational wind turbine rotors. Results show the significant effect of the turbine tower rotation, due to wave action, on the

[*]Corresponding Author, Tel.: +1(514)6633944;
E-mail address: saeidfadaeinaeini@cmail.carleton.ca

aeroelastic stability of the blades. Furthermore, it is shown that coupled motion of the platform as a rigid body with rotor angular velocity can lead to flutter instability at low wind speeds.

Keywords: *Floating wind turbine, Flutter, Non-uniform blade*

Nomenclature

A	Blade cross-sectional area
$\boldsymbol{A}$	Space state matrix
a	Quarter-chord length
b	Semi-chord length
$b_i(x)$	Generalized coordinates of bending
c	Chord length
$\boldsymbol{C}$	Damping matrix
$d_i(x)$	Generalized coordinates of torsion
e	Mass centroid offset from elastic axis
e_A	Tensile axis (area centroid) offset from elastic axis
E	Young's modulus
G	Shear modulus
$I_{\acute{y}}$	Blade cross-section moment of inertia about $\acute{y}$ axis
$I_{\acute{z}}$	Blade cross-section moment of inertia about $\acute{z}$ axis
J	Torsional rigidity
k_m	Radius of gyration of blade cross section
$\boldsymbol{i}, \boldsymbol{j}, \boldsymbol{k}$	Unit vectors associated with the undeformed blade coordinate system
$\boldsymbol{i}', \boldsymbol{j}', \boldsymbol{k}'$	Unit vectors associated with the deformed blade coordinate system

$\boldsymbol{I}, \boldsymbol{J}, \boldsymbol{K}$	Fixed unit vectors
$\boldsymbol{K}$	Stiffness matrix
l	Tower height
L	Lift force
m	Mass per unit length
M	Aerodynamic moment
$\boldsymbol{M}$	Mass matrix
N	Number of modes
$\boldsymbol{q}$	Generalized coordinates vector
Q_w, Q_φ	Generalized forces associated with w and φ
$\boldsymbol{Q}_{nc}$	Vector of generalized forces
$\boldsymbol{r}$	Position vector of an arbitrary point on the undeformed blade
$\boldsymbol{r}_1$	Position vector of the hub center in XYZ coordinate system
$\boldsymbol{r}_2$	Position vector of an arbitrary point on the blade after deformation
R	Blade length
t	Time
T	Kinetic energy
$\boldsymbol{T}$	Rotational matrix from XYZ to xyz
u, v, w	Elastic displacement in the x, y and z directions, respectively
U	Strain energy
$\boldsymbol{V}$	Velocity vector
$w_i(x)$	Bending mode shapes

x, y, z	Undeformed blade coordinate system
$\acute{x}, \acute{y}, \acute{z}$	Deformed blade coordinate system
x_1, y_1, z_1	Coordinates of a point on the deformed blade
X, Y, Z	Fixed coordinate system
$\boldsymbol{Z}$	State space coordinates vector
α	Angle of attack
γ	Angle of the blade relative to the fixed coordinate system
$\delta(\ )$	Variation of ( )
$\varepsilon_{11}, \varepsilon_{12}, \varepsilon_{13}$	Strain tensor components
$\varepsilon_{xx}, \varepsilon_{x\eta}, \varepsilon_{x\zeta}$	Engineering strain components
θ	Pre-twist angle
ρ	Density of the homogeneous model material
ρ_∞	Density of air
$C(k\ )$	Theodorsen's function
$\sigma_{xx}, \sigma_{x\eta}, \sigma_{x\zeta}$	Engineering stress components
φ	Elastic twist
$\varphi_i(x)$	Torsional mode shapes
Ω	Rotor angular velocity
$\Omega_x, \Omega_y, \Omega_z$	Angular velocities of tower base in X, Y and Z directions, respectively
$\boldsymbol{\Omega}_B$	Angular velocity vector of the turbine tower base
$\boldsymbol{\Omega}_R$	Blade angular velocity vector
$\boldsymbol{\Omega}_t$	Total angular velocity vector

$\dot{(\,)}$ $\partial/\partial t$

$\acute{(\,)}$ $\partial/\partial x$

1. Introduction

Horizontal-axis wind turbines (HAWT) are complex load-carrying structures which are subjected to non-conservative forces. In conventional onshore wind turbines, detecting and controlling the aeroelastic instabilities, such as blade flutter have been studied by various researchers. Floating wind turbines are a more recent innovation for capturing wind energy in offshore sites. Due to a number of prevailing meteorological and geographical factors present on open waters, such as continuous high-velocity winds and large available water surfaces that are located away from population centers, thus avoiding concerns about acoustic and visual disturbances by the public, the use of floating HAWTs have been on the rise. Indeed, these wind turbines are effective for capturing energy from strong and persistent offshore winds.

Nowadays, lightweight, strong, and durable materials are used by designers for wind turbine parts. Use of these materials in structurally optimized designs lead to more compliant wind turbine structures. Due to the resulting structural flexibility, aeroelastic analysis has become one of the most important aspects of wind turbine design. With the development of modern flexible wind turbine blades, these aeroelastic behaviors have received widespread attention in the research community and new technologies are now employed by designers to delay the onset of and overcome aeroelastic instabilities and corresponding vibrations.

Wind turbine dynamics, and aeroelasticity in general, is a practical problem which has been investigated by the research community. Several papers have been published in the field of wind turbines but available literature on flutter performance of floating offshore wind turbines, which

are susceptible to large blade deformation, is very limited. Lobitz worked on the aeroelastic response of bend–twist coupled blades for a 20 KW HAWT. He illustrated that stronger coupling between bending and twisting can result in more flutter occurrence. However, he assumed that the bending and torsional stiffnesses of the blade during flutter analysis remain unchanged [1]. Owens et al. developed the BLAST tool with some similarity to Lobitz's approach. They modified the structural modeling to include varying stiffness, mass, and damping matrices to account for aerodynamic and rotational effects [2]. Taehyoun Kim investigated the large static deflection of a nonlinear composite rotor blade by considering large amplitude structural and aeroelastic behavior of the blade [3]. Lee et al. considered a horizontal-axis wind turbine as a flexible multibody system and analyzed its dynamic behavior [4]. Hansen et al. surveyed the state of the art in wind turbine aerodynamic and aeroelasticity in 2006 [5]. The aerodynamic and structural modeling of the wind turbine and coupling between these two aspects were presented in their work. Larsen et al. analyzed the random and nonlinear vibration of wind turbine blades by means of Monte Carlo simulation [6]. They modeled the blades as a rotating Euler-Bernoulli beams with geometrical and inertial nonlinearities. The nacelle displacement was assumed to act as a harmonic and narrow-banded excitation on the blade. Shakya et al. carried out a parametric study to investigate the effect of unbalances resulting from the layup sequences for different parts of a composite wind turbine blade on the onset of flutter instability. In their model, both angle orientation and ply thickness were considered to be varied for various parts of the blade [7].

Lee et al. studied the operation and aeroelastic properties of the blades in HAWT with flexible dynamic components and presented an aerodynamic model based on Modified Strip Theory [8]. Mo et al. in 2015 presented an aeroelastic coupling analysis of the flexible blade of a large scale

HAWT [9]. They used the super element (SE) method for exact modeling of turbine blades and obtained time responses and stability boundaries for a 5 MW offshore HAWT.

Leble and Barakos presented an advanced method for simulating offshore HAWTs. They used Computational Fluid Dynamics (CFD), multibody dynamics, and smoothed particle hydrodynamics to simulate the wind turbine motions while modeling the mooring cables as springs and dampers [10]. Abdel Hafeez et al. presented a new aeroelastic model by considering the edgewise, flapwise, torsional, and extensional motions of a pretwisted, isolated and isotropic wind turbine blade in order to investigate the aeroelastic stability under normal conditions [11]. They conducted a parametric analysis to find out the effects of a blade's sectional offset, rotor speed, and wind speed on aeroelastic stability margin whilst taking into account the chordwise offset between mass, shear center, and aerodynamic center. Rafiee et al. performed an aeroelastic analysis of a full-scale composite wind turbine blade using its 3D model. They determined aerodynamic loading by using modified blade element momentum (BEM) theory and employed the CFD method for verification [12]. Kecskemety and Mcnamara focused on a comprehensive verification and validation of the NREL FAST code, which was enhanced to include a free vortex wake model [13]. The verification and validation were carried out through a comparison of blade lift distribution, wind turbine power, and force and moment coefficients using a combination of CFD and experimental data. Wang et al. presented the state-of-the-art aeroelastic modeling of wind turbine blades [14]. They discussed the advantages and disadvantages of different turbine blade models. Also, an overview of aeroelastic tools for wind turbines was conducted by Ageze et al. and opportunities for the future research directions in this field were indicated [15]. They employed an NREL 5 MW wind turbine blade to compare several aeroelastic codes. Recently, Liu et al. described a numerical tool based on the open-source CFD toolbox OpenFOAM for application to

floating offshore wind turbines (FOWT) [16]. They first modeled various benchmark cases to demonstrate the capability of the tool and then examined the effects of the dynamic motions of the floating platform on the wind turbine aerodynamic performance and also the impact of the wind turbine aerodynamics on the behavior of the floating platform.

Although extensive research has been carried out to investigate aeroelastic and dynamic responses of HAWTs, it appears that analytical aeroelastic stability analysis of HAWTs and specifically floating offshore wind turbines has not received much attention in the literature. To enrich the aforementioned bulk of literature in this field, the aeroelastic modeling and flutter analysis of a floating 5 MW HAWT blade is considered in this study. To this end, the wind turbine blade is modeled as a non-uniform flexible beam, the geometrically exact beam theory (GEBT) is employed to model the rotating blade connected to the tower, and its geometric and physical properties are extracted for an NREL offshore 5 MW wind turbine blade. Furthermore, discussions about the effects of tower base rotations in conjunction with airflow on the flutter speed and frequency of both parked and operational rotors are presented.

2. Problem statement

In the current study, a 5 MW wind turbine, as shown in Fig. 1, is considered. The turbine blades are considered to be cantilever beams with axially-varying structural properties. Combined flapwise and torsion flexibility is considered for this model. The wind turbine tower is assumed as a rigid beam whose tower base has three rotational degrees of freedom: roll, pitch and yaw.

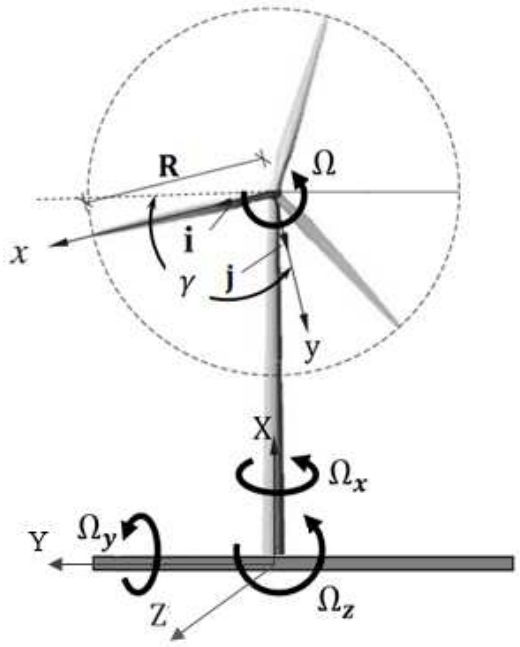

Figure 1. A schematic of wind turbine and selected coordinates.

Several coordinate systems are used to obtain the equations of motion. As shown in Fig. 1, the orthogonal axes X, Y, and Z are fixed at the tower root. The unit vectors of this system are $\boldsymbol{I}, \boldsymbol{J},$ and $\boldsymbol{K}$. This coordinate system rotates with respect to the inertial frame with angular velocities Ω_X, Ω_Y, and Ω_Z respectively. Another coordinate system is the blade coordinate system, *xyz*, with unit vectors $\boldsymbol{i}$, $\boldsymbol{j}$, and $\boldsymbol{k}$ in which the x axis lies along the length of the undeformed blade. The third coordinate system, $x'y'z'$ with unit vectors $\boldsymbol{i}', \boldsymbol{j}'$ and $\boldsymbol{k}'$ is fixed on the deformed blade which is shown in Fig. 2. After deformation, the shear center of the blade cross section, located at x, is displaced an amount v in the y direction and w in the z direction. Furthermore, the twist angle of the cross section changes from θ about the x axis to $\theta + \varphi$ about the x' axis.

The coordinate transformations that are needed consist of a simple transformation from $\boldsymbol{I}, \boldsymbol{J}, \boldsymbol{K}$ to $\boldsymbol{i}, \boldsymbol{j}, \boldsymbol{k}$ and a more complex transformation from $\boldsymbol{i}, \boldsymbol{j}, \boldsymbol{k}$ to $\boldsymbol{i}', \boldsymbol{j}', \boldsymbol{k}'$. These are used to derive the aeroelastic governing equations. For deriving the kinetic energy of the blade, the angular velocity

vector must be first transformed into the blade coordinate system, xyz. For a rotation γ of xy with respect to XY, the transformation matrix between the two coordinate systems is.

$$T = \begin{bmatrix} \cos(\gamma) & -\sin(\gamma) & 0 \\ \sin(\gamma) & \cos(\gamma) & 0 \\ 0 & 0 & 1 \end{bmatrix} \tag{1}$$

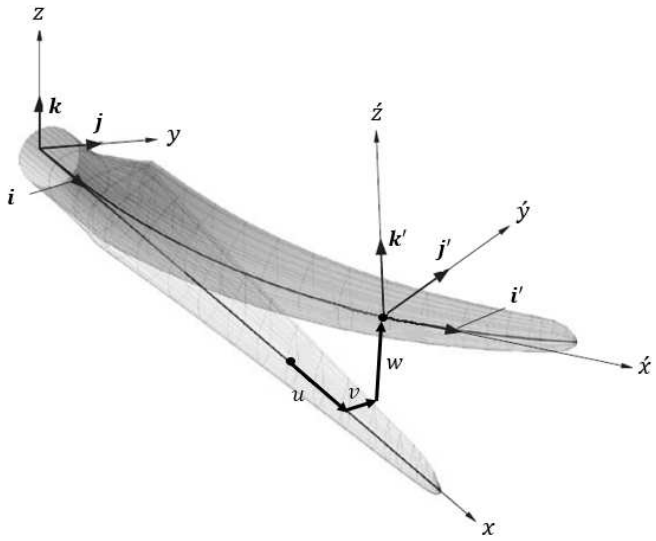

Figure 2. Undeformed and deformed blade coordinate systems.

Also, the transformation from $x'y'z'$ to xyz is expressed as [17]

$$\begin{aligned} \boldsymbol{i}' &= \left(1 - (1/2)w'^2\right)\boldsymbol{i} + w'\boldsymbol{k} \\ \boldsymbol{j}' &= -w'\sin(\theta+\varphi)\,\boldsymbol{i} + \cos(\theta+\varphi)\,\boldsymbol{j} + \left(1 - (1/2)w'^2\right)\cos(\theta+\varphi)\,\boldsymbol{k} \\ \boldsymbol{k}' &= -w'\cos(\theta+\varphi)\,\boldsymbol{i} + \sin(\theta+\varphi)\,\boldsymbol{j} + \left(1 - (1/2)w'^2\right)\cos(\theta+\varphi)\,\boldsymbol{k} \end{aligned} \tag{2}$$

3. Equations of motion

Equations of motion are derived using the Ritz method and Lagrange equations that may be expressed as

$$\mathrm{d}/\mathrm{d}t\,(\partial L/\partial \dot{\boldsymbol{q}}) - \partial L/\partial \boldsymbol{q} = \boldsymbol{Q}_{nc} \tag{3}$$

In this equation L is the Lagrangian which is defined as

$$L = T - U \tag{4}$$

where T and U are kinetic and strain energy, respectively. Also $\boldsymbol{q}$ is the vector of generalized coordinates vector and $\boldsymbol{Q_{nc}}$ is the vector of generalized forces.

3.1 Work and Energy Terms

The strain energy of the blade can be expressed as

$$U = (1/2)\int_0^R \iint_A (\sigma_{xx}\varepsilon_{xx} + \sigma_{x\eta}\varepsilon_{x\eta} + \sigma_{x\zeta}\varepsilon_{x\zeta})\,d\eta d\zeta dx \tag{5}$$

where η and ζ are cross-sectional local coordinates, and σ_{ij} and ϵ_{ij} are stress and strain components, respectively. Following [17] in Eq. (5), stress and strain components are related as follows

$$\begin{aligned} \sigma_{xx} &= E\varepsilon_{xx} \\ \sigma_{x\eta} &= E\varepsilon_{x\eta} \\ \sigma_{x\zeta} &= E\varepsilon_{x\zeta} \end{aligned} \tag{6}$$

while the engineering strain components are related to classic strain tensor components

$$\begin{aligned} \varepsilon_{xx} &= \varepsilon_{11} \\ \varepsilon_{x\eta} &= 2\varepsilon_{12} \\ \varepsilon_{x\zeta} &= 2\varepsilon_{13} \end{aligned} \tag{7}$$

Moreover, the classic strain components can be expressed in terms of blade deformations as follows

$$\varepsilon_{11} = \frac{1}{2}w'^2 + \frac{1}{2}(\eta^2 + \zeta^2)\varphi'^2 - w'' \times (\eta \sin(\theta + \varphi) + \zeta \cos(\theta + \varphi))$$

$$\varepsilon_{12} = -\frac{1}{2}\zeta\varphi' \tag{8}$$

$$\varepsilon_{13} = \frac{1}{2}\eta\varphi'$$

By substituting these equations into Eq. (5), the strain energy can be recast as

$$U = (1/2)\int_0^R [(1/2)EAw'^4 + (1/4)\varphi'^4(EI_{y'}(x) + EI_{z'}(x)) + EI_{z'}(x)\varphi'^2 w''^2$$
$$+EI_{y'}(x)w''^2 + (1/2)(EI_{y'}(x) + EI_{z'}(x))\varphi'^2 w'^2 - EAe_A\dot{\varphi}w'^2 w'' \tag{9}$$
$$-E\overset{*}{B}_2\varphi'^2 w'' + GJ(x)\varphi'^2]\mathrm{d}x$$

Where A and E are the cross-sectional area and modulus of elasticity of the blade, respectively; $I_{y'}$ and $I_{z'}$ are the blade cross-section moments of inertia about the y' and z' axes, respectively; J is the torsional rigidity constant; and e_A is the tensile axis (area centroid) offset from the elastic axis.

Blade kinetic energy can be expressed as

$$T = (1/2)\int_0^R \iint_A \rho\, \boldsymbol{V}\cdot\boldsymbol{V}\mathrm{d}\eta\mathrm{d}\zeta\mathrm{d}x \tag{10}$$

where ρ is the blade density and $\boldsymbol{V}$ is the velocity vector of an arbitrary point on the turbine blade. The position vector of such a point can be expressed as

$$\boldsymbol{r} = \boldsymbol{r}_1 + \boldsymbol{r}_2 \tag{11}$$

where $\boldsymbol{r_1}$ is the position vector of the hub center in the XYZ coordinate system and $\boldsymbol{r_2}$ is the position vector of an arbitrary point on the blade after deformation expressed in the xyz coordinate system. These vectors are

$$\boldsymbol{r_1} = l\boldsymbol{I}$$
$$\boldsymbol{r}_2 = x_1\boldsymbol{i} + y_1\boldsymbol{j} + z_1\boldsymbol{k} \tag{12}$$

where l is the height of the wind turbine tower and x_1, y_1 and z_1 can be obtained as [17]

$$x_1 = x - w'(\eta \sin(\theta + \varphi) + \zeta \cos(\theta + \varphi))$$
$$y_1 = \eta \cos(\theta + \varphi) - \zeta \sin(\theta + \varphi) \quad (13)$$
$$z_1 = w + (\eta \sin(\theta + \varphi) + \zeta \cos(\theta + \varphi))$$

Now, the velocity vector $\boldsymbol{V}$ of any point on the blade can be obtained using the transport theorem as

$$\boldsymbol{V} = \mathrm{d}\boldsymbol{r}/\mathrm{d}t = \mathrm{d}\boldsymbol{r_1}/\mathrm{d}t + \mathrm{d}\boldsymbol{r_2}/\mathrm{d}t = (\partial \boldsymbol{r_1}/\partial t + \boldsymbol{\Omega_B} \times \boldsymbol{r_1}) + (\partial \boldsymbol{r_2}/\partial t + \boldsymbol{\Omega_t} \times \boldsymbol{r_2}) \quad (14)$$

where $\boldsymbol{\Omega_B}$ is the turbine base angular velocity and $\boldsymbol{\Omega_t}$ is total angular velocity which is the sum of the base and blade angular velocity vectors. So,

$$\boldsymbol{\Omega_B} = \Omega_x \boldsymbol{I} + \Omega_y \boldsymbol{J} + \Omega_z \boldsymbol{K}$$
$$\boldsymbol{\Omega_t} = \boldsymbol{\Omega_B} + \boldsymbol{\Omega_R} \quad (15)$$

where

$$\boldsymbol{\Omega_R} = \Omega \boldsymbol{k} \quad (16)$$

Substituting Eqs. (11-16) into Eq. (10), blade kinetic energy can be written as

$$\begin{aligned} T = (1/2) \int_0^R [m(x)((\dot{w} - l\Omega_y - x\Omega_y \cos(\gamma) + x\Omega_x \sin(\gamma))^2 + (x(\Omega + \Omega_z) \\ -w\Omega_y \sin(\gamma) + l\Omega_z \cos(\gamma) - w\Omega_x \cos(\gamma))^2 + (w\Omega_y \cos(\gamma) \\ -w\Omega_x \sin(\gamma) + l\Omega_z \sin(\gamma))^2) - (x(\Omega + \Omega_z) - w\Omega_y \sin(\gamma) \\ +l\Omega_z \cos(\gamma) - w\Omega_x \cos(\gamma))^2 - (\dot{w} - l\,\Omega_y + x\Omega_x \sin(\gamma) \\ -x\Omega_y \cos(\gamma))^2 - (w\Omega_y \cos(\gamma) - w\Omega_x \sin(\gamma) \\ +l\Omega_z \sin(\gamma))^2 + (\dot{w} - l\Omega_y - \Omega_y \cos(\gamma)(x - m(x)ew' \sin(\theta(x) + \varphi)) \\ +\Omega_x \sin(\gamma)(x - m(x)ew' \sin(\theta(x) + \varphi)) + m(x)\, e\dot{\varphi} \cos(\theta(x) + \varphi) \\ + m(x)\, e\, \Omega_x \cos(\theta(x) + \varphi) \cos(\gamma) + m(x)\, e\, \Omega_y \cos(\theta(x) + \varphi) \sin(\gamma))^2 \end{aligned} \quad (17)$$

$$+(\Omega_x \cos(\gamma)(w + m(x)e \sin(\theta(x) + \varphi))$$

$$-(x - m(x)ew' \sin(\theta(x) + \varphi))(\Omega + \Omega_z)$$

$$+\Omega_y \sin(\gamma)(w + m(x)e \sin(\theta(x) + \varphi))$$

$$-l\Omega_z \cos(\gamma) + m(x)e\varphi \sin(\theta(x) + \varphi))^2$$

$$+(\Omega_x \sin(\gamma)(w + m(x)e \sin(\theta(x) + \varphi))$$

$$-\Omega_y \cos(\gamma)(w + m(x)e \sin(\theta(x) + \varphi))$$

$$-l\Omega_z \sin(\gamma) + m(x)e\dot{w}' \sin(\theta(x) + \varphi)$$

$$+m(x)e \cos(\theta(x) + \varphi)(\Omega + \Omega_z) + m(x)ew'\dot{\varphi} \cos(\theta(x) + \varphi))^2]\mathrm{d}x$$

The vector of generalized forces $\boldsymbol{Q_{nc}}$ in Eq. (3) can be obtained by means of the principal of virtual work. The virtual work of non-conservative forces acting on the blade may be expressed as

$$\delta W = \int_0^R (-L\,\delta w + M\delta\phi)\mathrm{d}x \tag{18}$$

where L and M are the aerodynamic lift force and moment, respectively. Also, δw and $\delta\varphi$ are flapwise bending and torsion virtual displacements of the blade. It should be mentioned that since the main objective of this study was to investigate the effect of the base rotation on the flutter boundary of the blade, considering the relatively low values of the rotor angular velocity, the centrifugal forces in the blades could be neglected as a first approximation.

The BEM theory was used to model the total aerodynamic loads in this study [18–20]. The BEM theory is a well-established theory in the literature and we did not want to consume valuable space in paper by describing it in detail.

Meanwhile the lift and moment loads at each segment are calculated using Theodorsen's Unsteady Theory [21]. In this vein, the aerodynamic lift L and moment M are expressed as

$$L = 2\pi\rho_\infty VbC(k)[\dot{w} + V\varphi + b(\frac{1}{2} - a)\dot{\varphi}] + \pi\rho_\infty b^2(\ddot{w} + V\dot{\varphi} - ba\ddot{\varphi})$$
$$M = -\pi\rho_\infty b^2[\frac{1}{2}\ddot{w} + V\dot{\varphi} + b(\frac{1}{8} - \frac{a}{2})\ddot{\varphi}] \quad (19)$$

where ρ_∞ is the density of air, b is semi-chord length, $C(k)$ is a complex-valued function of the reduced frequency k, V is the fluid velocity, and a is the quarter-chord length. The velocity components acting on the blade airfoil section are depicted in Fig. 3 [22].

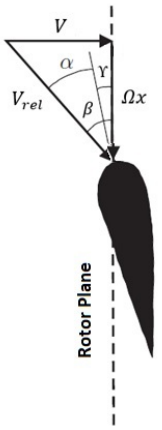

Figure 3. Velocity components acting on the blade airfoil section.

Based on Theodorsen's theory and the abovementioned velocity components, the angle of attack is obtained as [22]

$$\alpha = C(k)[\varphi + \frac{\Omega x}{V} + \frac{\dot{w}}{V} + \frac{b}{V}(\frac{1}{2} - a)\dot{\varphi}] \quad (20)$$

Lobitz [23] confirmed that flutter speeds obtained from a quasi-steady analysis are more conservative than those obtained by using the unsteady form of Theodorsen's theory. As such, a quasi-steady analysis is used in this study where in Theodorsen's theory C(k) is considered to be equal to unity. Hence, the aerodynamic lift and moments applied at each blade section are modified to be [22]

$$L = 2\pi\rho_\infty Vb[\dot{w} + \frac{\Omega x}{V} + V(\theta + \varphi) + b(\frac{1}{2} - a)\dot{\varphi}] + \pi\rho_\infty b^2(\ddot{w} + V\dot{\varphi} - ba\ddot{\varphi})$$
$$M = -\pi\rho_\infty b^2[\frac{1}{2}\ddot{w} + V\dot{\varphi} + b(\frac{1}{8} - \frac{a}{2})\ddot{\varphi}] \quad (21)$$

1

2 **3.2 Physical and Geometrical Properties of the Blade**

3 Due to the complexity of wind turbine blades, in many cases, uniform beam models are used in
4 their aeroelastic analysis. However, such models are limited in their ability to represent real wind
5 turbine blades that have geometry that varies nonlinearly along their span. For a reliable analysis
6 of turbine blades, it is necessary to develop refined models to account for the effects of geometrical
7 and physical nonuniformities.

8 To this end, in this research the blade of a NREL 5 MW HAWT is considered for the aeroelastic
9 analysis. All physical and geometrical properties of the blade, including its mass per unit length,
10 pre-twist angle, cross sectional area, mass moments of inertia, and chord length are considered to
11 vary along its span as distributed parameters that are shown in Table 1. It is important to note
12 that in this study, the pre-twist angle of the blade has been considered, while in previous papers
13 thus has been ignored for the sake of simplicity of the structural model. Additionally, the focus
14 of the study described in this paper is mainly on investigation of those parameters which
15 influence the flutter instability, such as the angular velocity of the tower as well as rotor speed.
16 The effects of parameters, like pitch angle, which can mitigate aeroelastic instabilities were not
17 the focus of this study. Moreover, since in the reference NREL 5 MW wind turbine the peak of
18 the power coefficient curve occurs at TSR of 7.55 at a rotor-collective blade-pitch angle of 0.0
19 degrees [24], the focus of this article is on extracting the maximum power while having a
20 constant blade pitch angle and investigation of different TSRs on the starting point of the flutter
21 instability.

Table 1. Blade structural properties distributed over the blade span [24].

Radius (*m*)	BMassDen (*kg/m*)	StrcTwst (*deg*)	FlpStff (*N.m^2*)	EdgStff (*N.m^2*)	GJStff (*N.m^2*)	FlpIner (*Kg.m*)	EdgIner (*Kg.m*)
1.5	678.935	13.308	1.81E+10	1.81E+10	5.56E+09	972.86	973.04
1.7	678.935	13.308	1.81E+10	1.81E+10	5.56E+09	972.86	973.04
2.7	773.363	13.308	1.94E+10	1.96E+10	5.43E+09	1091.52	1066.38
3.7	740.55	13.308	1.75E+10	1.95E+10	4.99E+09	966.09	1047.36
4.7	740.042	13.308	1.53E+10	1.98E+10	4.67E+09	873.81	1099.75
5.7	592.496	13.308	1.08E+10	1.49E+10	3.47E+09	648.55	873.02
6.7	450.275	13.308	7.23E+09	1.02E+10	2.32E+09	456.76	641.49
7.7	424.054	13.308	6.31E+09	9.14E+09	1.91E+09	400.53	593.73
8.7	400.638	13.308	5.53E+09	8.06E+09	1.57E+09	351.61	547.18
9.7	382.062	13.308	4.98E+09	6.88E+09	1.16E+09	316.12	490.84
10.7	399.655	13.308	4.94E+09	7.01E+09	1.00E+09	303.6	503.86
11.7	426.321	13.308	4.69E+09	7.17E+09	8.56E+08	289.24	544.7
12.7	416.82	13.181	3.95E+09	7.27E+09	6.72E+08	246.57	569.9
13.7	406.186	12.848	3.39E+09	7.08E+09	5.47E+08	215.91	601.28
14.7	381.42	12.192	2.93E+09	6.24E+09	4.49E+08	187.11	546.56
15.7	352.822	11.561	2.57E+09	5.05E+09	3.36E+08	160.84	468.71
16.7	349.477	11.072	2.39E+09	4.95E+09	3.11E+08	148.56	453.76
17.7	346.538	10.792	2.27E+09	4.81E+09	2.92E+08	140.3	436.22
19.7	339.333	10.232	2.05E+09	4.50E+09	2.61E+08	124.61	398.18
21.7	330.004	9.672	1.83E+09	4.24E+09	2.29E+08	109.42	362.08
23.7	321.99	9.11	1.59E+09	4.00E+09	2.01E+08	94.36	335.01
25.7	313.82	8.534	1.36E+09	3.75E+09	1.74E+08	80.24	308.57
27.7	294.734	7.932	1.10E+09	3.45E+09	1.44E+08	62.67	263.87
29.7	287.12	7.321	8.76E+08	3.14E+09	1.20E+08	49.42	237.06
31.7	263.343	6.711	6.81E+08	2.73E+09	8.12E+07	37.34	196.41
33.7	253.207	6.122	5.35E+08	2.55E+09	6.91E+07	29.14	180.34
35.7	241.666	5.546	4.09E+08	2.33E+09	5.75E+07	22.16	162.43
37.7	220.638	4.971	3.15E+08	1.83E+09	4.59E+07	17.33	134.83
39.7	200.293	4.401	2.39E+08	1.58E+09	3.60E+07	13.3	116.3
41.7	179.404	3.834	1.76E+08	1.32E+09	2.74E+07	9.96	97.98
43.7	165.094	3.332	1.26E+08	1.18E+09	2.09E+07	7.3	98.93
45.7	154.411	2.89	1.07E+08	1.02E+09	1.85E+07	6.22	85.78
47.7	138.935	2.503	9.09E+07	7.98E+08	1.63E+07	5.19	69.96
49.7	129.555	2.116	7.63E+07	7.10E+08	1.45E+07	4.36	61.41
51.7	107.264	1.73	6.11E+07	5.18E+08	9.07E+06	3.36	45.44
53.7	98.776	1.342	4.95E+07	4.55E+08	8.06E+06	2.75	39.57
55.7	90.248	0.954	3.94E+07	3.95E+08	7.08E+06	2.21	34.09
56.7	83.001	0.76	3.47E+07	3.54E+08	6.09E+06	1.93	30.12
57.7	72.906	0.574	3.04E+07	3.05E+08	5.75E+06	1.69	20.15
58.7	68.772	0.404	2.65E+07	2.81E+08	5.33E+06	1.49	18.53
59.2	66.264	0.319	2.38E+07	2.62E+08	4.94E+06	1.34	17.11
59.7	59.34	0.253	1.96E+07	1.59E+08	4.24E+06	1.1	11.55
60.2	55.914	0.216	1.60E+07	1.38E+08	3.66E+06	0.89	9.77
60.7	52.484	0.178	1.28E+07	1.19E+08	3.13E+06	0.71	8.19
61.2	49.114	0.14	1.01E+07	1.02E+08	2.64E+06	0.56	6.82
61.7	45.818	0.101	7.55E+06	8.51E+07	2.17E+06	0.42	5.57

62.2	41.669	0.062	4.60E+06	6.43E+07	1.58E+06	0.25	4.01
62.7	11.453	0.023	2.50E+05	6.61E+06	2.50E+05	0.04	0.94
63	10.319	0	1.70E+05	5.01E+06	1.90E+05	0.02	0.68

In Table 1, the first column refers to the location along the blade's pitch axis with the succeeding columns to the right, respectively, indicating the distributed blade section mass per unit length, structural-twist angle, flapwise and edgewise section stiffness, blade torsion stiffness, and the flapwise and edgewise section inertia [24].

Fig. 4 shows, as an example, the variation of the flap inertia, edge inertia, and mass per unit length along the blade [24].

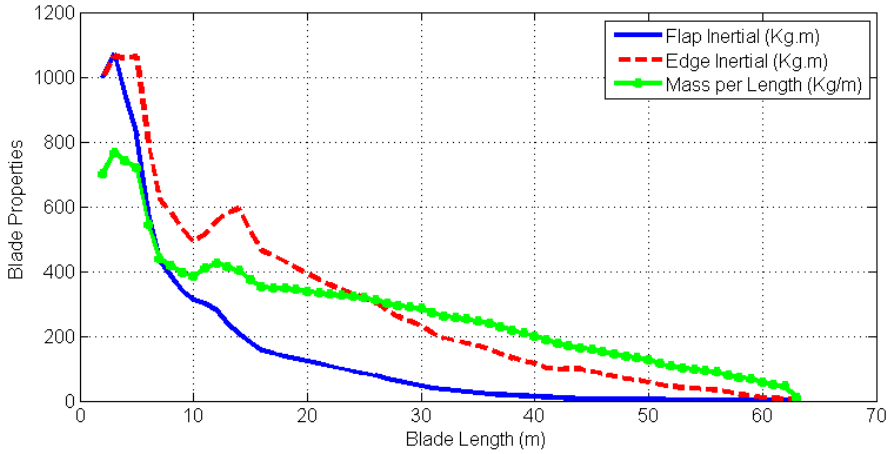

Figure 4. Variation of the flap inertia, edge inertia and mass per unit length along the blade span [24].

It can be seen from this figure that the blade properties change substantially along its span. Therefore, for accurate modeling of the blade, its geometrical and physical properties must be considered to be functions of the span-wise coordinate x. To achieve this, for each property a mathematical function is fit to the series of data points obtained for the NREL 5 MW turbine blade. Fig. 5 shows, as an example, the curve fitting process to obtain the blade pre-twist angle as a function of the span-wise coordinate x.

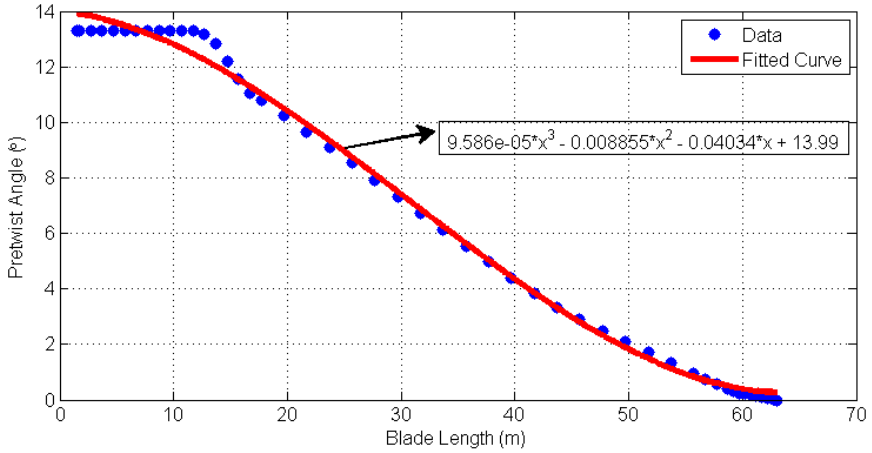

Figure 5. Blade pre-twist angle as a function of span and curve-fitted function.

Using the same procedure, the following geometrical and physical properties of the blade can be obtained as

$$m(x) = -1.579 \times 10^{-5}\, x^5 + 0.00294x^4 - 0.2054x^3 + 6.615x^2 - 103.2x + 976.2$$

$$EI_y(x) = -393.2x^5 + 7.625 \times 10^4 x^4 - 5.616 \times 10^6 x^3 + 1.962 \times 10^8 x^2 - 3.385 \times 10^9 x + 2.752 \times 10^{10}$$

$$EI_z(x) = -536.1x^5 + 1.01 \times 10^5 x^4 - 7.229 \times 10^6 x^3 + 2.455 \times 10^{84} x^2 - 4.025 \times 10^9 x + 2.738 \times 10^{10}$$

$$GJ(x) = -142x^5 + 2.784 \times 10^4 x^4 - 2.087 \times 10^6 x^3 + 7.445 \times 10^7 x^2 - 1.266 \times 10^9 x + 8.376 \times 10^9 \quad (22)$$

$$mk_{m_1}^2(x) = -2.433 \times 10^{-5} x^5 + 0.004636x^4 - 0.3376x^3 + 11.79x^2 - 202.6x + 1479$$

$$mk_{m_2}^2(x) = -1.96 \times 10^{-5} x^5 + 0.003504x^4 - 0.2351x^3 + 7.51x^2 - 129x + 1344$$

$$\theta(x) = 9.586 \times 10^{-5} x^3 - 0.008855x^2 - 0.04034x + 13.99$$

$$c(x) = -2.78 \times 10^{-6} x^4 + 4.0 \times 10^{-4} x^3 - 0.0206x^2 + 0.386x + 2.26$$

where $mk_{m_1}^2(x)$ and $mk_{m_2}^2(x)$ are the flapwise and edgewise mass moment of inertia values, EI_z and EI_y are the flapwise and edgewise sectional stiffnesses, $\theta(x)$ is the blade pre-twist angle, and $c(x)$ is the blade chord [24].

3.3 Discretized Aeroelastic Governing Equations

To extract the discretized form of the blade equations of motion, the Ritz method is applied to the kinetic and strain energy terms. To this end, w and φ are represented as

$$w(x,t) = \sum_{i=1}^{N} w_i(x) b_i(t)$$
$$\varphi(x,t) = \sum_{i=1}^{N} \varphi_i(x) d_i(t) \tag{23}$$

where N is the number of modes and $w_i(x)$ and $\varphi_i(x)$ are the bending and torsional mode shapes, respectively; and $b_i(t)$ and $d_i(t)$ are their corresponding modal coordinates. The following family of spatial functions is used here [21]

$$w_i(x) = ((x/R)^{1+i}\{6 + i^2(1-(x/R))^2 + i(5 - 6(x/R) + (x/R)^2)\})/(i(i+1)(i+2)(i+3)) \tag{24}$$
$$\varphi_i(x) = \sin(\,(2i+1)\pi x/2R)$$

Substituting Eqs. (22-24) into Eqs. (9, 17) and employing the resulting equations in Lagrange's Equation (Eq. (3)), finally leads to a set of coupled ordinary differential equations in the standard form

$$\boldsymbol{M\ddot{q} + C\dot{q} + Kq = Q_{nc}} \tag{25}$$

where $\boldsymbol{M}$, $\boldsymbol{K}$, $\boldsymbol{C}$ and $\boldsymbol{Q_{nc}}$ denote the mass matrix, stiffness matrix, damping matrix, and non-conservative load vector, respectively, while $\boldsymbol{q}$ is the overall vector of the generalized coordinates,

$$\boldsymbol{q} = \{\boldsymbol{b_i}^T \boldsymbol{d_i}^T\}^T \tag{26}$$

4. Solution Methodology

Due to the intricate and complex coupling of generalized coordinates which are involved in the aeroelastic governing equations it is difficult to find their closed form solution; and as mentioned previously, the solution is searched by using an approximate solution procedure based on the Ritz method.

In this paper, flutter analysis of an offshore wind turbine blade is carried out in both the locked (stopped) and unlocked (rotating) rotor conditions. There are some differences between the aeroelastic analyses in these two situations.

4.1 Flutter Boundary Detection for Parked Rotors

Floating wind turbines can be affected by different weather conditions. In the case of extreme weather disturbances and severe sea states it is necessary to lock the turbine rotor. The flutter boundary, in this situation, can be detected by eigenvalue analysis. To this end, Eq. (25) reduces to a set of first-order coupled ordinary differential equations (ODE) as

$$\dot{\boldsymbol{Z}} = [\boldsymbol{A}]\boldsymbol{Z} \tag{27}$$

where the system matrix $[\boldsymbol{A}]$ and the state vector $\boldsymbol{Z}$, are

$$[\boldsymbol{A}] = \begin{bmatrix} [\boldsymbol{0}] & [\boldsymbol{I}] \\ -[\boldsymbol{M}]^{-1}[\boldsymbol{K}] & -[\boldsymbol{M}]^{-1}[\boldsymbol{C}] \end{bmatrix} \tag{28}$$

$$\boldsymbol{Z} = \{\boldsymbol{q}^{\mathrm{T}}\ \dot{\boldsymbol{q}}^{\mathrm{T}}\}^T \tag{29}$$

The problem is now reduced to that of determining the eigenvalues of matrix $[\boldsymbol{A}]$ at a given air speed. The flutter speed is calculated through an iteration procedure to determine the speed at which the real part of the complex eigenvalues become zero.

4.2 Flutter Boundary Detection for Operational Rotors

For operational rotors, the rotors are unlocked and their angular speed Ω is not zero. In this case, because of the relation $\gamma = \Omega t$, the time term enters directly into the aeroelastic governing equations of the blade and the aforementioned eigenvalue analysis cannot be used in the flutter analysis. In this situation, time response analysis is used to detect the flutter boundary. The flutter is determined as a boundary between dynamically stable and unstable conditions and corresponds to simple harmonic motion. To identify the flutter speed, the time response of the blade for each operational condition is examined as the wind speed increases. The wind speed at which the amplitude of tip vibration grows in an unbounded fashion corresponds to a flutter velocity that identifies the starting point of the flutter instability of the system. Flutter frequency is obtained using Fast Fourier Transform (FFT) analysis on the system time response at the flutter condition.

5. Results and Discussion

Six bending modes and six torsion modes are considered in the Ritz method to develop the discretized form of the aeroelastic governing equations. Pertinent data for the particular floating wind turbine used here are given in Table 2. Due to the wind direction, the value of the pitch rotation (rotational velocity of the tower about the Y direction) is selected to be greater than the value of the rotational velocity of the tower in the other two directions.

Sea conditions are defined by the combination of wind and wave characteristics and are very much dependent upon the geographic location, season, local prevailing weather conditions, and recent weather in areas from which storm waves propagate. As a result of these complexities and the fact that the sea state, characterized by significant wave height and modal period, are not exclusively linked to the local wind speed, there is no consistent mapping between sea conditions and turbine angular velocities. For that reason, the angular velocity of the rotor is set in the operating range of the HAWT. In this research, the effect of periods of constant rotational speed on the flutter boundary has been studied. This is an important step in the future analysis of time-varying base motions. Moreover, proper consideration of the time varying base motion requires accurate information about the relationship between the conditions of the waves and the base motions, which is the subject of much ongoing research.

Table 2. Floating wind turbine parameters.

Parameter	Value
Rotational velocity of the tower about the X axis (Ω_X)	0.5 rad/s
Rotational velocity of the tower about the Y axis (Ω_Y)	1.0 rad/s
Rotational velocity of the tower about the Z axis Ω_Z)	0.5 rad/s
Rotational velocity of the rotor (Ω)	0 rad/s
Angle of the blade relative to the fixed coordinate system (γ)	0 degree
Tower height of turbine (l)	87.6 m

5.1 Verification

To verify the accuracy of the model developed in this investigation, results in the absence of the aerodynamic loads are compared with the corresponding results obtained using the ABAQUS software package. To this end, the geometric properties of an NREL 5 MW wind turbine blade are

modeled exactly using the CATIA software package. Using this geometrical data, the surface points of each blade section are obtained. The blade geometrical model is finally extracted by entering the coordinates of surface points in the CATIA software. The final model of the blade is shown in Fig. 6 (a). In order to verify the theoretical results, the model is imported to ABAQUS. In ABAQUS, the blade is considered as a solid blade and the beam properties are assigned to it and then, by using vibration analysis, natural frequencies of the blade are obtained. Fig. 6 (b) shows the first flapwise bending mode of the blade.

Table 3 compares the results from the developed model with those obtained by ABAQUS. The low percentage differences between the two results demonstrate the accuracy of the present model. The small differences between the two sets of results come from the fact that in the developed model, curve-fitted functions are used for the blade properties while in the ABAQUS analysis, the exact geometrical inertial characteristics were simulated. The effect of this difference appears to become more discernable for the first twisting frequency.

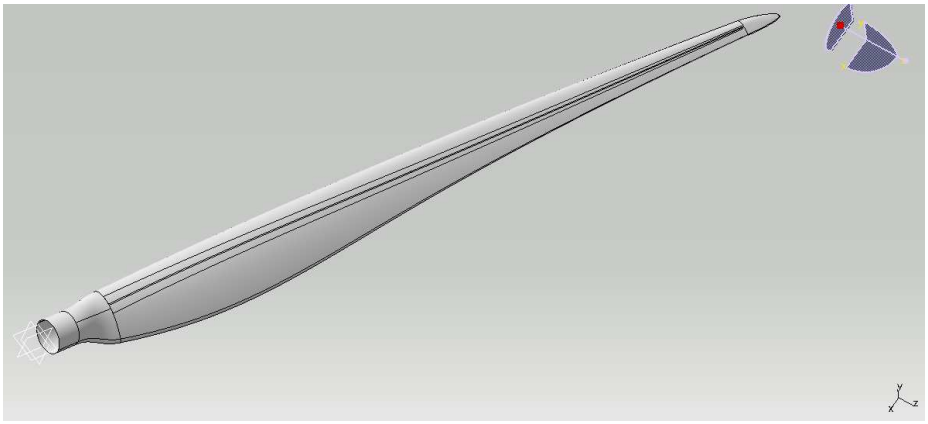

(a)

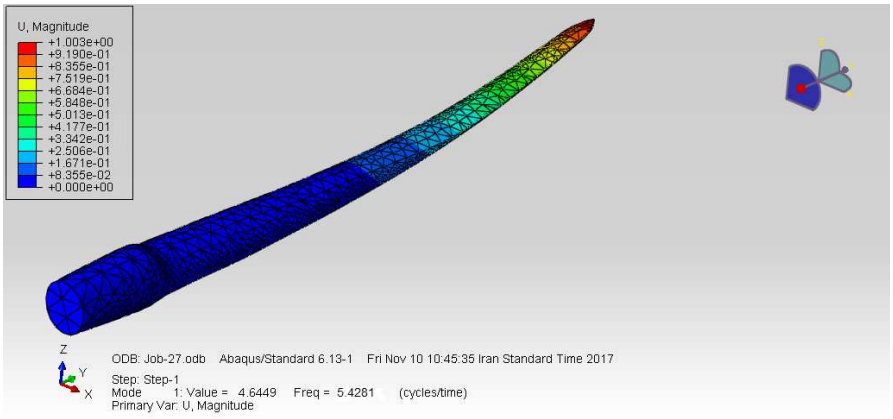

(b)

Figure 6. (a) The blade final model in CATIA, (b) The first bending mode in ABAQUS.

Table 3. Comparison of the results from the model with ABAQUS software solutions.

Frequency Mode	Current Study	ABAQUS	Difference (%)
First bending frequency (rad/s)	5.31	5.43	2.21
Second bending frequency (rad/s)	17.41	17.84	2.41
First twisting frequency (rad/s)	6.75	6.01	12.31
Second twisting frequency (rad/s)	31.22	30.05	3.75

Additionally, for the purpose of model verification, results for a non-uniform rotating beam are compared in Table 4 with Ref. [25] with good agreement.

Table 4. Comparison between the results.

Frequency Mode	Current Study	**Ref.** [25]	Error Percentage
First Bending Mode (rad/s)	5.32	5.55	4.14
Second Bending Mode (rad/s)	20.15	20.87	3.45

Moreover, our results of flutter in the fixed support condition and in the presence of aerodynamic loads are also comparable to the results obtained by Gao et al [26] as shown in Table 5.

Table 5. Comparison between the flutter results for fixed foundation status

Flutter Condition	**Current Study**	**Ref.** [26]	**Error Percentage**
Flutter Speed (m/s)	117.11	103.01	12.04
Flutter Frequency (rad/s)	5.31	5.68	-6.96

5.2 Floating Wind Turbine with Parked Rotors

As noted before, in severe environmental conditions the rotors of HAWTs are usually locked to avoid any potential damage. In these conditions, the high sea state can create significant angular velocities of the floating wind turbine tower. Effects of these angular velocities on the flutter boundary of parked turbine blades are examined in this section.

The effect of the angular velocity of the tower Ω_X on flutter velocity and frequency of the blade is shown in Fig. 7. It can be seen from this figure that increasing Ω_X decreases both the flutter speed and frequency. Although Ω_X does not affect the flutter boundary in a significant manner, it affects the flutter frequency considerably. Increasing Ω_X from 1 to 5 rad/s decreases U_f by 1.62% and w_f by 66.35%. The effects of the tower angular velocities Ω_y and Ω_z on flutter velocity and frequency of the turbine blade are shown in Figs. 8 and 9, respectively. Fig. 8, in which $\Omega_X = \Omega_Z = 0$, indicates that increasing Ω_Y will decrease the flutter speed and frequency dramatically. This can be considered as an important factor in floating wind turbine design, since Ω_Y can destabilize the blades and lead to flutter at lower speeds.

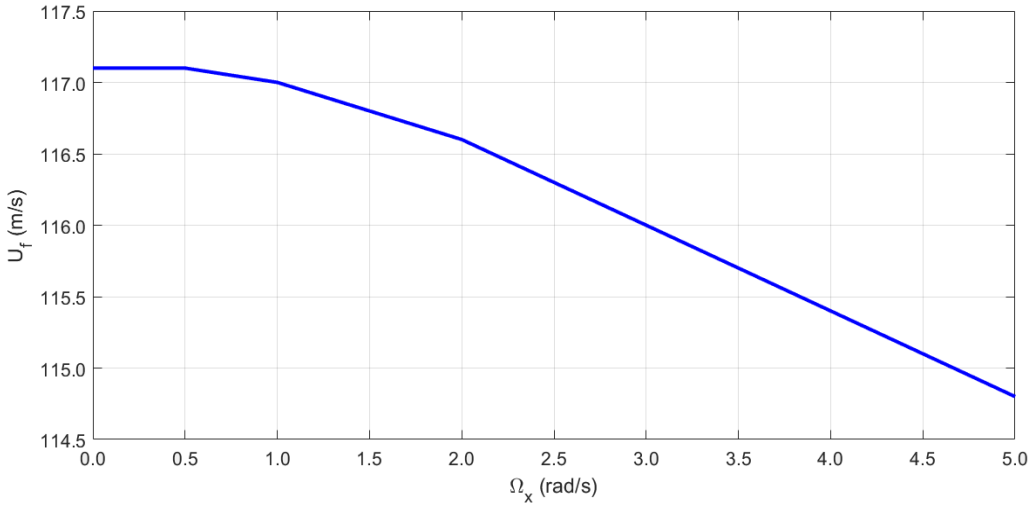

(a)

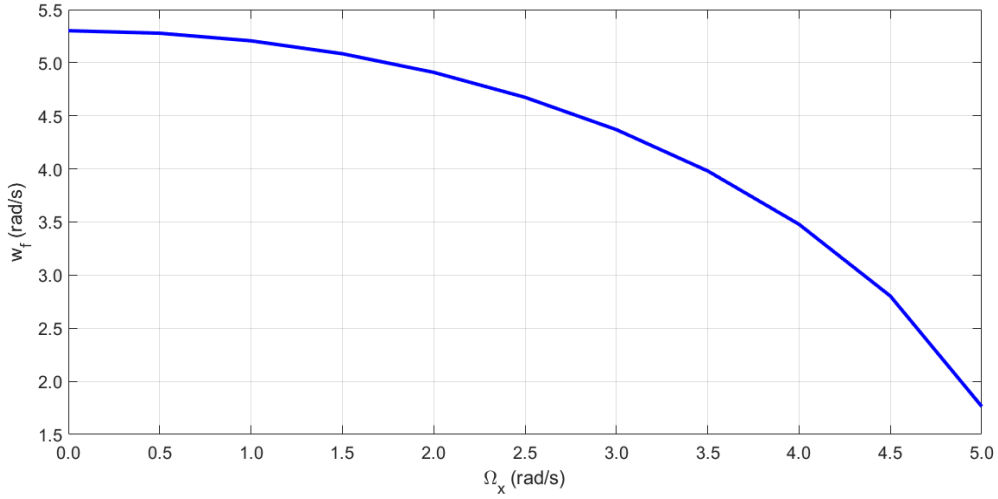

(b)

Figure 7. Effects of the tower angular velocity Ω_X of parked rotor blades on (a) flutter velocity, U_f; and (b) flutter frequency, w_f.

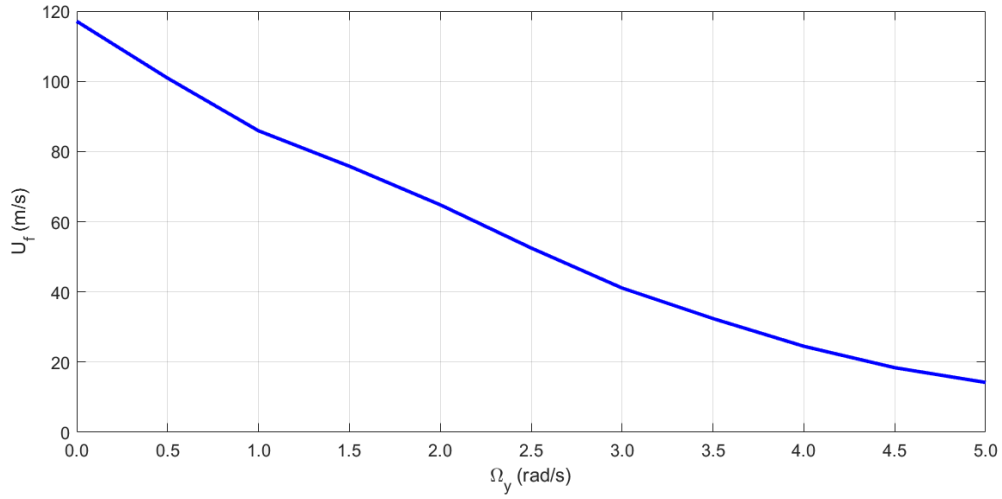

(a)

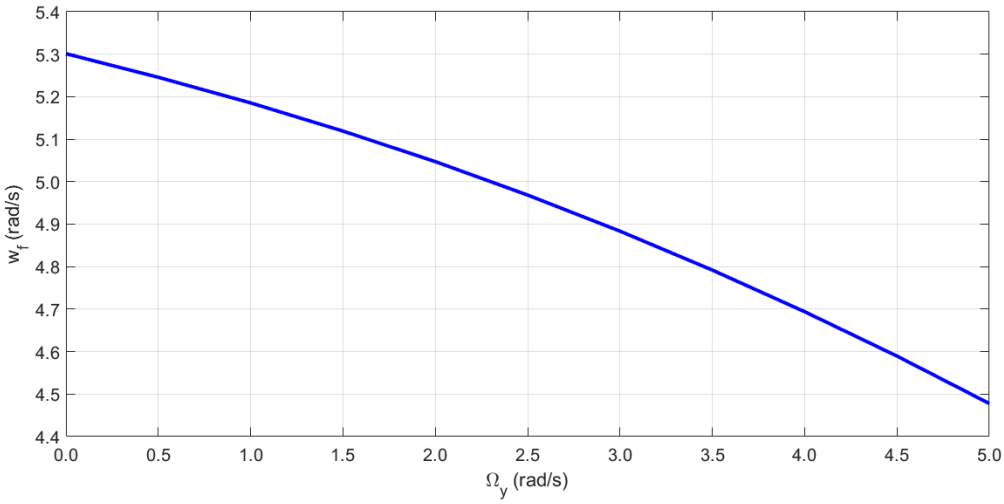

(b)

Figure 8. Effect of the tower angular velocity Ω_y of parked rotor blades on (a) flutter velocity, U_f; and (b) flutter frequency, w_f.

Fig. 9 also shows the stability boundary when Ω_x and Ω_y equal zero and only Ω_Z acts on the tower base. A continued decrease in the flutter speed accompanying the increase in Ω_Z is observed. It can be concluded that large waves in the *Y* direction that cause large rotation of the tower about

the Z axis decrease the stability boundary of the turbine blades. So, it is concluded that generation of angular velocities Ω_y and Ω_Z at the tower base have significant effects on limiting the stability region of the turbine blades.

Fig. 10 shows the effects of the simultaneous presence of angular velocities of the tower in the Y and Z directions on flutter velocity and frequency of the blades. In this case $\Omega_X = 0$ and $\Omega_Y = \Omega_Z$. This situation may be faced in atmospheric conditions in which the sea is turbulent, and waves excite the floating wind turbine tower base in multiple directions simultaneously.

Results indicate that an increase of wave-induced angular velocities of the tower base can induce a lower flutter speed and frequency. This means that the angular velocity of the base decreases the aeroelastic stability region of the turbine blades. For large values of these angular velocities, the diagram may coincide with the zero-velocity line which means that the base angular velocity leads to instability even in the absence of air flow.

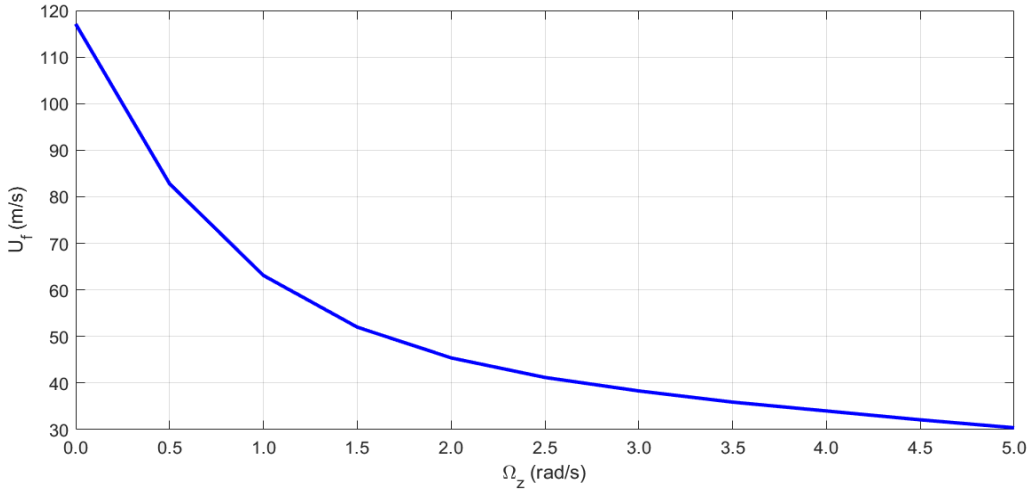

(a)

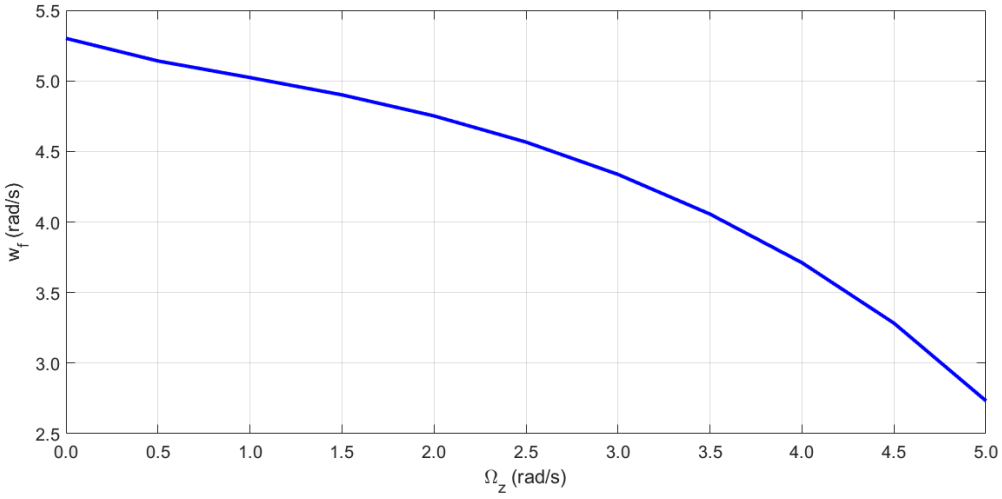

(b)

Figure 9. Effect of the tower angular velocity Ω_z of parked rotor blades on (a) flutter velocity, U_f; and (b) flutter frequency, w_f.

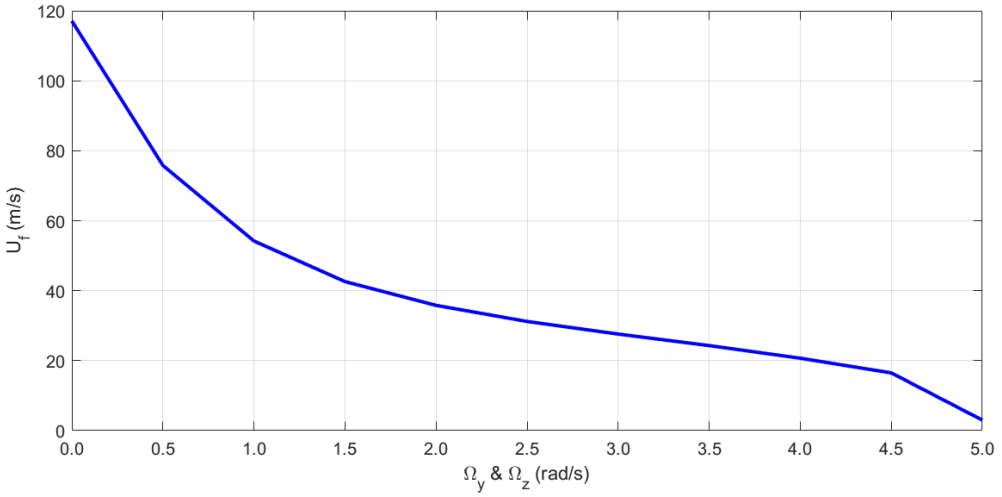

(a)

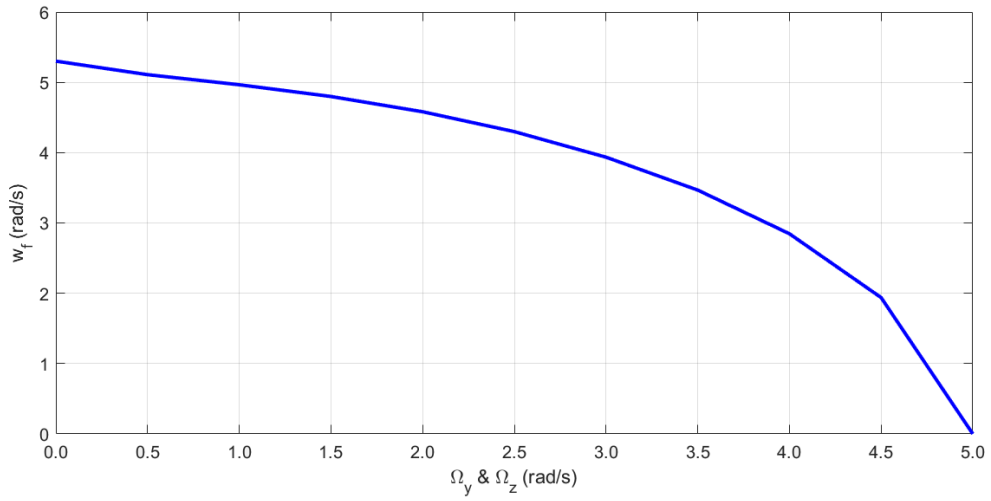

(b)

Figure 10. Effect of simultaneous presence of tower angular velocities Ω_y and Ω_z for parked rotor blades on (a) flutter velocity; and (b) flutter frequency.

Table 6 summarizes results of the flutter analysis of the wind turbine blades in the parked rotor condition. It can be seen that Ω_Y and Ω_Z have a more significant effect on the flutter boundary that the flutter frequency.

Table 6. Summary of the aeroelastic results for a wind turbine with parked rotors.

Rotational velocity of tower	**Flutter Velocity (m/s)**	**Flutter Frequency (rad/s)**
$\Omega_X = 1\ (\mathrm{rad/s})\ ,\ \Omega_Y = \Omega_Z = 0$	117.1	5.2
$\Omega_X = 1\ (\mathrm{rad/s})\ ,\ \Omega_Y = \Omega_Z = 0.5\ (\mathrm{rad/s})$	76.5	5.0
$\Omega_Y = 1\ (\mathrm{rad/s})\ ,\ \Omega_X = \Omega_Z = 0$	94.9	5.2
$\Omega_Z = 1\ (\mathrm{rad/s})\ ,\ \Omega_X = \Omega_Y = 0$	63.1	5.0
$\Omega_Y = \Omega_Z = 1\ (\mathrm{rad/s})\ ,\ \Omega_X = 0$	54.2	4.9

5.3 Floating Wind Turbines with Operational Rotors

In this section, the common mode of wind turbine operation in which rotor blades rotate due to wind loads is investigated. Combined effects of the floating tower angular velocity and rotor angular velocity have potential to significantly change the flutter stability boundary of the blades. Fig. 11 demonstrates the influence of the rotor angular velocity Ω on the flutter speed and frequency of the blade for different values of the tower base angular velocity in the X direction. In this case, tower base angular velocities in other directions are equal to zero. Results show that increasing the rotor angular velocity decreases the flutter speed and plays a destabilizing role in the dynamic stability of the blade.

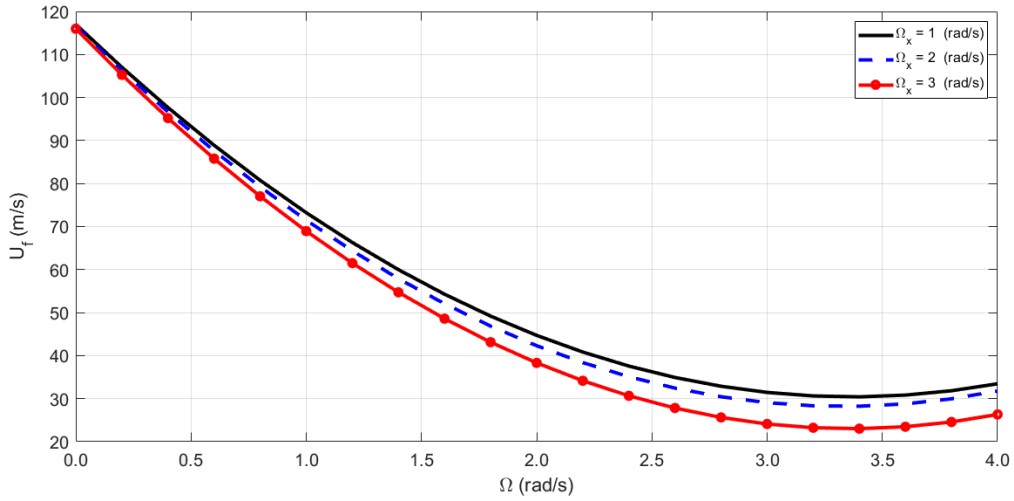

(a)

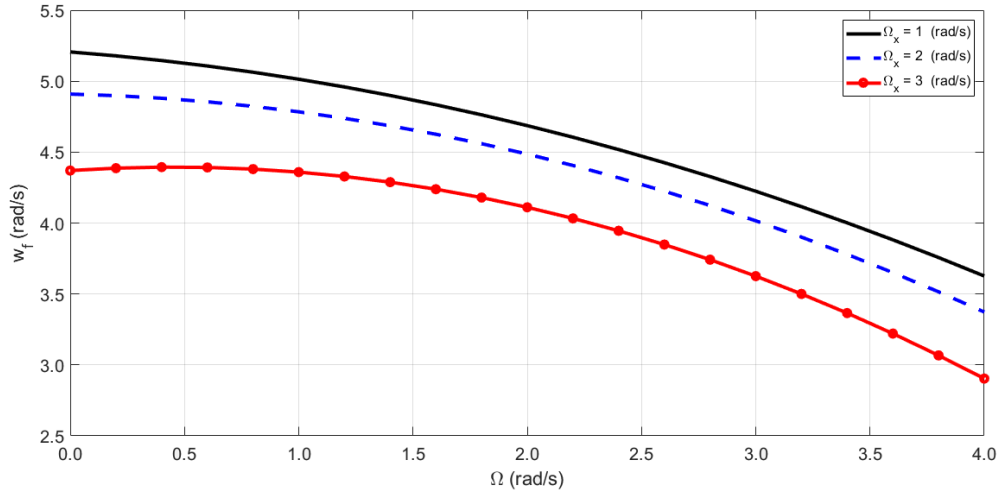

(b)

Figure 11. The effect of changing the rotational velocity of the rotors in the presence of rotational velocity Ω_x on (a) flutter velocity; and (b) flutter frequency.

Effects of the tower base angular velocity in the Y direction on flutter velocity and frequency of the turbine blade for two selected values of the rotor angular velocity are presented in Fig. 12. It can be seen that increasing the angular velocity of the rotor will increase the risk of flutter occurrence, and instability occurs at lower wind speed compared to the parked rotor condition. Furthermore, Ω_Y has a destabilizing effect on the turbine blades and increasing it leads to flutter at lower speeds.

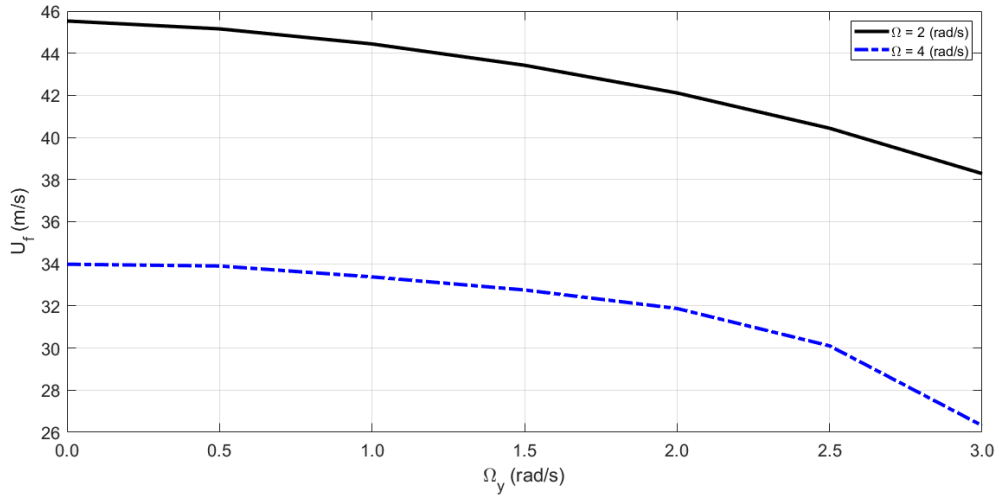

(a)

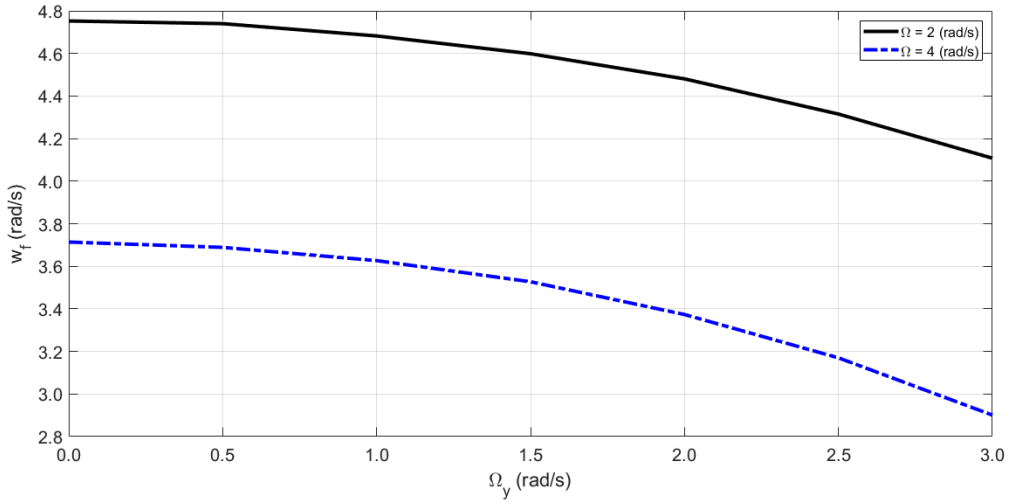

(b)

Figure 12. The effect of changing the rotational velocity of the rotors in the presence of rotational velocity Ω_y on (a) flutter velocity; and (b) flutter frequency.

Fig. 13 indicates the influence of rotor velocity on flutter velocity and the frequency of the blades for three different values of the tower angular velocity in the Z direction. In this case, $\Omega_Y = \Omega_X = 0$. Results show that increasing the rotor angular velocity decreases the blade's flutter speed and frequency. This is more apparent for higher values of Ω_Z.

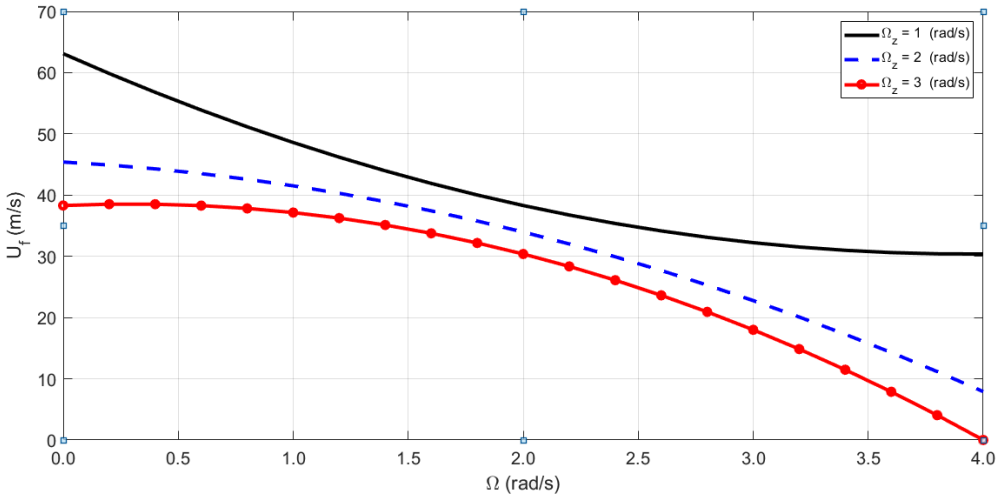

(a)

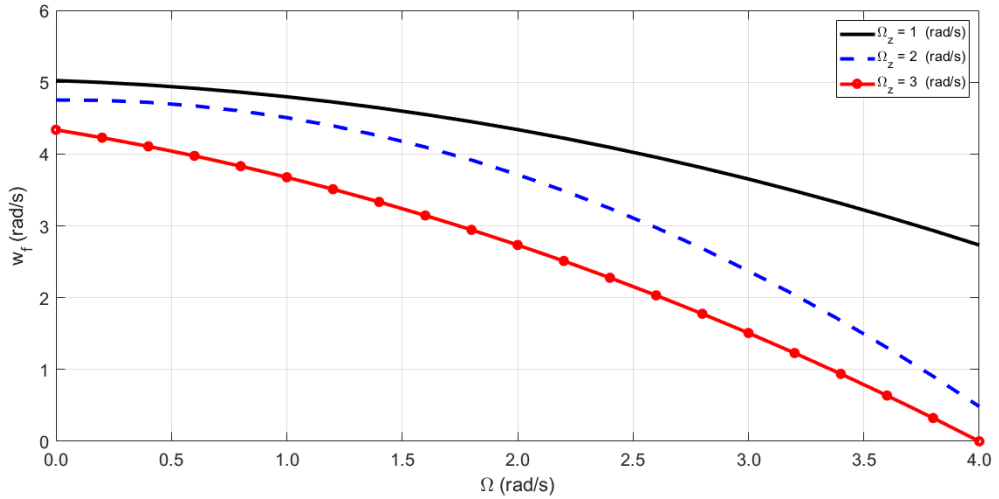

(b)

Figure 13. The effect of changing the rotational velocity of the rotors in the presence of rotational velocity Ω_z on (a) flutter velocity; and (b) flutter frequency.

The effect of combined Ω_y and Ω_z angular velocities on flutter speed and frequency for operational rotor blades for two selected values of Ω are plotted in Fig. 14. In this case, $\Omega_X = 0$ and the tower base is impacted by waves in the *Y* and *Z* directions, simultaneously. It can be seen that increasing the rotor angular velocity limits the aeroelastic stability region of the blades. Furthermore, results show a continued decrease in flutter speed and frequency accompanies the increase in the tower

base angular velocities. It appears that at lower values of Ω, as Ω_x and Ω_y increase, the corresponding decreases in flutter speed and frequency are less pronounced than at higher values of Ω.

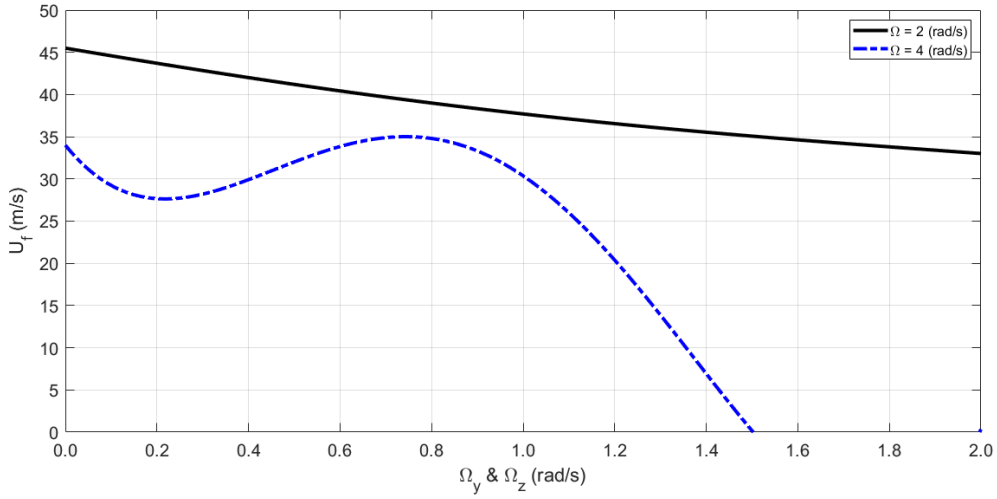

(a)

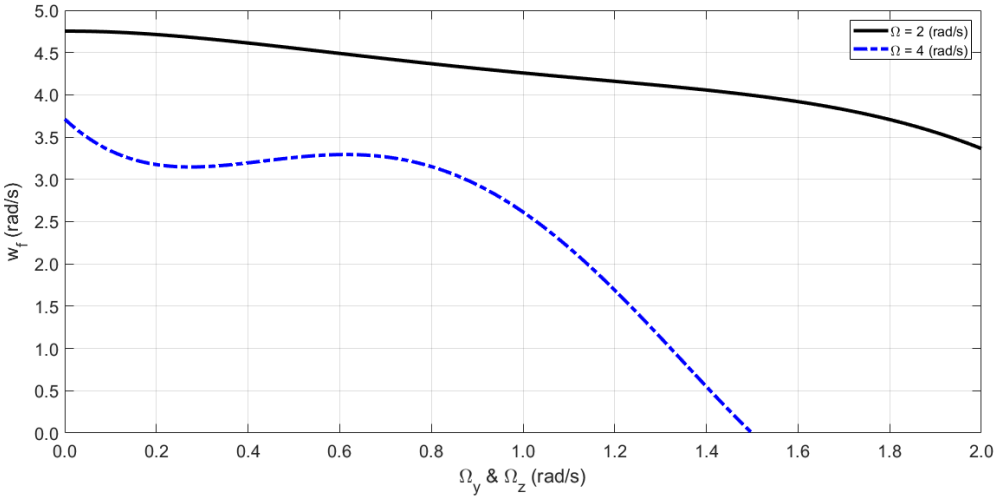

(b)

Figure 14. Effects of the simultaneous tower angular velocities Ω_y and Ω_z on (a) flutter velocity; and (b) flutter frequency for operational rotor blades for two selected values of Ω.

Finally, a summary of aeroelastic analysis results for floating wind turbines with operational rotors subjected to various tower base angular velocities is shown in Table 7. Results show the important effect of the angular velocity of the tower base of floating HAWTs on the blades' flutter boundary.

Table 7. The summary of the aeroelastic results for wind turbines with operational rotors

Rotor velocity	Rotation velocity of tower	Flutter Velocity (m/s)	Flutter Frequency (rad/s)
$\Omega = 2$ (rad/s)	$\Omega_X = 1$ (rad/s) , $\Omega_Y = \Omega_Z = 0$	44.7	4.7
	$\Omega_X = 1$ (rad/s) , $\Omega_Y = \Omega_Z = 0.5$ (rad/s)	40.5	4.5
	$\Omega_Y = 1$ (rad/s) , $\Omega_X = \Omega_Z = 0$	44.2	4.7
	$\Omega_Z = 1$ (rad/s) , $\Omega_X = \Omega_Y = 0$	38.3	4.3
	$\Omega_Y = \Omega_Z = 1$ (rad/s) , $\Omega_X = 0$	37.7	4.3
$\Omega = 4$ (rad/s)	$\Omega_X = 1$ (rad/s) , $\Omega_Y = \Omega_Z = 0$	33.4	3.6
	$\Omega_X = 1$ (rad/s) , $\Omega_Y = \Omega_Z = 0.5$ (rad/s)	31.4	3.2
	$\Omega_Y = 1$ (rad/s) , $\Omega_X = \Omega_Z = 0$	33.4	3.6
	$\Omega_Z = 1$ (rad/s) , $\Omega_X = \Omega_Y = 0$	30.4	2.7
	$\Omega_Y = \Omega_Z = 1$ (rad/s) , $\Omega_X = 0$	30.3	2.6

6. Conclusion

Aeroelastic modeling and flutter of the blades of a floating HAWT is considered in this study. The blade is modeled as a nonuniform bending-torsion flexible beam and its geometric and physical properties are extracted from an NREL 5MW wind turbine blade. Forces and lift due to angular rotation of the base, as well as moments due to aerodynamic loads are included in the blade aeroelastic governing equations.

A parametric study of base angular velocity on the flutter speed and frequency of both parked rotors and operational rotors is presented. Results show that the base angular velocity has a detrimental effect on flutter onset and restricts the blades' dynamic stability region. Results suggest that increasing the base angular velocity always seems to lower the flutter speed and frequency. Simultaneous generation of angular velocities Ω_y and Ω_Z at the tower base has the most significant effect on limiting the stability region of turbine blades. In the case of operational rotors, combination effects of the rotor and tower base rigid body motions lead to blade instability at lower wind speeds compared to the parked rotor condition.

References

[1] Lobitz, D.W., Veers, P.S.: Aeroelastic behavior of twist-coupled hawt blades. In: 1998 ASME Wind Energy Symposium. pp. 75–83. American Institute of Aeronautics and Astronautics Inc, AIAA (1998)

[2] Owens, B.C., Griffith, D.T., Resor, B.R., Hurtado, J.E.: Impact of Modeling Approach on Flutter Predictions for Very Large Wind Turbine Blade Designs. In: Proceedings of the American Helicopter Society 69th Annual Forum (2013)

[3] Kim, T.: Nonlinear large amplitude structural and aeroelastic behavior of composite rotor blades at large static deflection, (1992)

[4] Lee, D., Hodges, D.H., Patil, M.J.: Multi-flexible-body Dynamic Analysis of Horizontal Axis Wind Turbines. Wind Energy. 5, 281–300 (2002). https://doi.org/10.1002/we.66

[5] Hansen, M.O.L., Sørensen, J.N., Voutsinas, S., Sørensen, N., Madsen, H.A.: State of the art in wind turbine aerodynamics and aeroelasticity. Prog. Aerosp. Sci. 42, 285–330 (2006). https://doi.org/10.1016/j.paerosci.2006.10.002

[6] Larsen, J.W., Iwankiewicz, R., Nielsen, S.R.K.: Nonlinear stochastic stability analysis of wind turbine wings by Monte Carlo simulations. Probabilistic Eng. Mech. 22, 181–193 (2007). https://doi.org/10.1016/j.probengmech.2006.11.002

[7] Shakya, P., Sunny, M.R., Maiti, D.K.: A parametric study of flutter behavior of a composite wind turbine blade with bend-twist coupling. Compos. Struct. 207, 764–775 (2019). https://doi.org/10.1016/j.compstruct.2018.09.064

[8] Lee, J.W., Lee, J.S., Han, J.H., Shin, H.K.: Aeroelastic analysis of wind turbine blades based on modified strip theory. J. Wind Eng. Ind. Aerodyn. 110, 62–69 (2012). https://doi.org/10.1016/j.jweia.2012.07.007

[9] Mo, W., Li, D., Wang, X., Zhong, C.: Aeroelastic coupling analysis of the flexible blade of a wind turbine. Energy. 89, 1001–1009 (2015). https://doi.org/10.1016/j.energy.2015.06.046

[10] Leble, V., Barakos, G.: Demonstration of a coupled floating offshore wind turbine analysis with high-fidelity methods. J. Fluids Struct. 62, 272–293 (2016). https://doi.org/10.1016/j.jfluidstructs.2016.02.001

[11] Hafeez, M.M.A., El-Badawy, A.A.: Flutter limit investigation for a horizontal axis wind turbine blade. J. Vib. Acoust. Trans. ASME. 140, 1–12 (2018). https://doi.org/10.1115/1.4039402

[12] Rafiee, R., Tahani, M., Moradi, M.: Simulation of aeroelastic behavior in a composite wind turbine blade. J. Wind Eng. Ind. Aerodyn. 151, 60–69 (2016). https://doi.org/10.1016/j.jweia.2016.01.010

[13] Kecskemety, K.M., McNamara, J.J.: Influence of wake dynamics on the performance and aeroelasticity of wind turbines. Renew. Energy. 88, 333–345 (2016).

https://doi.org/10.1016/j.renene.2015.11.031

[14] Wang, L., Liu, X., Kolios, A.: State of the art in the aeroelasticity of wind turbine blades: Aeroelastic modelling, (2016)

[15] Ageze, M.B., Hu, Y., Wu, H.: Wind Turbine Aeroelastic Modeling: Basics and Cutting Edge Trends. Int. J. Aerosp. Eng. 2017, (2017). https://doi.org/10.1155/2017/5263897

[16] Liu, Y., Xiao, Q., Incecik, A., Peyrard, C., Wan, D.: Establishing a fully coupled CFD analysis tool for floating offshore wind turbines. Renew. Energy. 112, 280–301 (2017). https://doi.org/10.1016/j.renene.2017.04.052

[17] Hodges, D.H., Dowell, E.H.: Nonlinear equations of motion for the elastic bending and torsion of twisted nonuniform rotor blades. (1974)

[18] Wang, T.: A brief review on wind turbine aerodynamics. Theor. Appl. Mech. Lett. 2, 062001 (2012). https://doi.org/10.1063/2.1206201

[19] Jeong, M.S., Kim, S.W., Lee, I., Yoo, S.J.: Wake impacts on aerodynamic and aeroelastic behaviors of a horizontal axis wind turbine blade for sheared and turbulent flow conditions. J. Fluids Struct. 50, 66–78 (2014). https://doi.org/10.1016/j.jfluidstructs.2014.06.016

[20] Hansen, M.O.L., Aagaard Madsen, H.: Review paper on wind turbine aerodynamics. J. Fluids Eng. Trans. ASME. 133, (2011). https://doi.org/10.1115/1.4005031

[21] Hodges, D.H., Pierce, G.A.: Introduction to Structural Dynamics and Aeroelasticity. Cambridge University Press, Cambridge (2011)

[22] Fadaei Naeini, S.: Aeroelastic Analysis of Wind Turbine with Movable Base, (2016)

[23] Lobitz, D.W.: Aeroelastic stability predictions for a MW-sized blade. Wind Energy. 7, 211–224 (2004). https://doi.org/http://doi.wiley.com/10.1002/we.120

[24] Jonkman, J., Butterfield, S., Musial, W., Scott, G.: Definition of a 5-MW Reference Wind

Turbine for Offshore System Development. , Golden, CO (2009)

[25] Tang, A.Y., Li, X.F., Wu, J.X., Lee, K.Y.: Flapwise bending vibration of rotating tapered Rayleigh cantilever beams. J. Constr. Steel Res. 112, 1–9 (2015). https://doi.org/10.1016/j.jcsr.2015.04.010

[26] Gao, Q., Cai, X., Guo, X. wen, Meng, R.: Parameter sensitivities analysis for classical flutter speed of a horizontal axis wind turbine blade. J. Cent. South Univ. 25, 1746–1754 (2018). https://doi.org/10.1007/s11771-018-3865-x